JACS
JOURNAL OF THE AMERICAN CHEMICAL SOCIETY
Article
pubs.acs.org/JACS

Hexagonal Graphene Onion Rings

Zheng Yan,[†] Yuanyue Liu,[‡,§] Jian Lin,[‡,§] Zhiwei Peng,[†] Gunuk Wang,[†] Elvira Pembroke,[†] Haiqing Zhou,[†,⊥] Changsheng Xiang,[†] Abdul-Rahman O. Raji,[†] Errol L. G. Samuel,[†] Ting Yu,*[,⊥] Boris I. Yakobson,*[,†,‡,§] and James M. Tour*[,†,‡,§]

[†]Department of Chemistry, [‡]Richard E. Smalley Institute for Nanoscale Science and Technology, and [§]Department of Mechanical Engineering and Materials Science, Rice University, 6100 Main Street, Houston, Texas 77005, United States

[⊥]Division of Physics and Applied Physics, School of Physical and Mathematical Sciences, Nanyang Technological University, Singapore 637371

Supporting Information

ABSTRACT: Precise spatial control of materials is the key capability of engineering their optical, electronic, and mechanical properties. However, growth of graphene on Cu was revealed to be seed-induced two-dimensional (2D) growth, limiting the synthesis of complex graphene spatial structures. In this research, we report the growth of onion ring like three-dimensional (3D) graphene structures, which are comprised of concentric one-dimensional hexagonal graphene ribbon rings grown under 2D single-crystal monolayer graphene domains. The ring formation arises from the hydrogenation-induced edge nucleation and 3D growth of a new graphene layer on the edge and under the previous one, as supported by first principles calculations. This work reveals a new graphene-nucleation mechanism and could also offer impetus for the design of new 3D spatial structures of graphene or other 2D layered materials. Additionally, in this research, two special features of this new 3D graphene structure were demonstrated, including nanoribbon fabrication and potential use in lithium storage upon scaling.

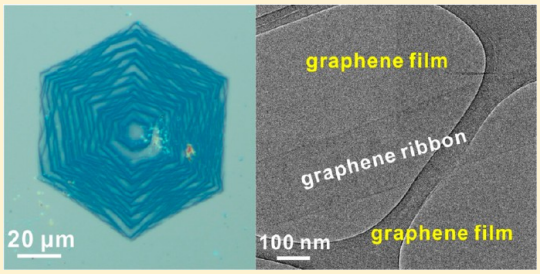

INTRODUCTION

Graphene provides unusual mechanical, optical, and electronic properties that can be influenced by its spatial structures.[1−3] Recent advancements in chemical vapor deposition (CVD) methods have enabled the large-scale production of two-dimensional (2D) graphene films on Cu substrates.[4−6] Meanwhile, several interesting graphene-based hybrid structures, such as h−BN−graphene,[7,8] graphene−CNTs,[9,10] CNT−graphene ribbons,[11] and graphene−graphane,[12] have been recently achieved by a two-step process. However, existing graphene growth methods on Cu have fundamental limitations that are based on a seed-induced 2D growth mechanism and do not allow one to fabricate *in situ* complex spatial graphene structures during the growth process.[13−16] In this research, it has been found that three-dimensional (3D) growth of new graphene layers on the edges of the original graphene layer could be induced by controlling H_2 partial pressure during the growth process. This stands as a complementary method to CVD growth while permitting growth of complex graphene-based spatial structures. By this method, onion ring like 3D hexagonal graphene structures (hexagonal graphene onion rings, HGoRs) were fabricated via the *in situ* growth of graphene ribbon rings on the edge and under hexagonal monolayer graphene domains. The structural models of HGoRs are displayed in Figure 1a, showing that the topside monolayer graphene domain (gray) and the bottomside few-layer graphene ribbons (blue) combine together to form an onion ring like pseudo-3D graphene structure.

One of the most promising applications of graphene lies in its potential use in field effect transistors, which has been hindered by the absence of an electronic bandgap.[17] Research has demonstrated that an energy gap could be introduced *via* shaping graphene into graphene nanoribbons (GNR), a graphene strip with fixed width.[17,18] Moreover, the electronic properties of GNRs have been revealed to depend on their widths and edges.[19] The widths of GNRs can be adjusted using different fabrication methods.[20−23] GNR edges can be stabilized *via* termination with non-C atoms, such as S.[11] The control of the twist and chirality of GNRs has been realized in recent research.[24,25] In this work, we demonstrate that GNRs can be made from HGoRs when the top layer graphene domain is removed using Ar plasma,[21] indicating a new bottom-up fabrication method of GNRs.

EXPERIMENTAL SECTION

Synthesis of HGoRs. Growth of HGoRs on Cu foils was achieved as follows. Cu foils were first cleaned using electrochemical-polishing and high-pressure annealing techniques.[16] The pretreated Cu was loaded into the CVD chamber and annealed for 30 min at 1074 °C with the flow rate of H_2 at 500 sccm and the chamber pressure at 500

Received: April 19, 2013
Published: July 2, 2013

   dx.doi.org/10.1021/ja403915m | J. Am. Chem. Soc. 2013, 135, 10755−10762

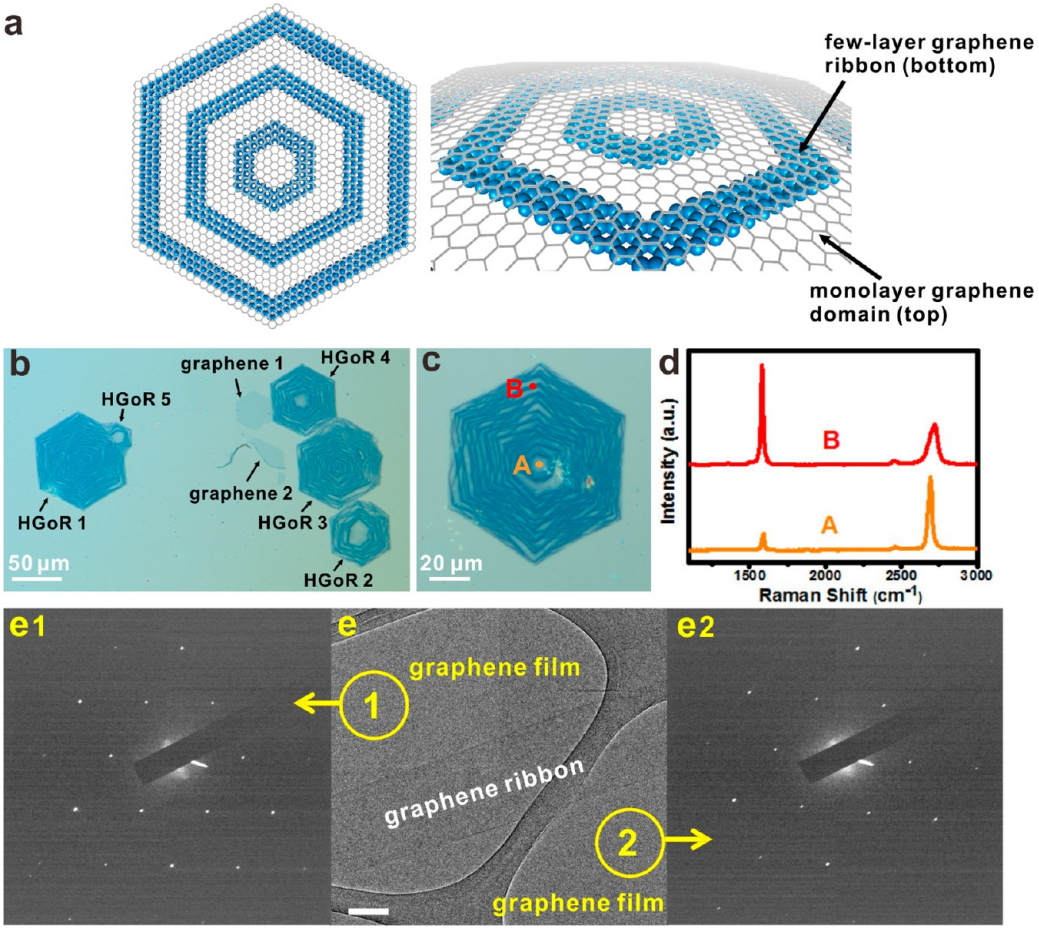

Figure 1. Synthesis and spectroscopic analysis of hexagonal graphene onion rings (HGoRs). (a) Top view and side view of the structural models of HGoR, which was a combination of the topside monolayer graphene domain (gray) and the bottomside few-layer graphene ribbons (blue). HGoRs are synthesized on Cu foils by heating in a H_2/CH_4 atmosphere at 1074 °C with the chamber pressure held at 500 Torr. (b and c) Typical optical images of as-produced HGoRs transferred onto SiO_2/Si wafers, showing blue graphene ribbon rings somewhat concentrically grow on or under lighter monolayer graphene domains. (d) Raman spectra of point A and point B in c. (e) SAED patterns and the TEM image of one HGoR transferred onto a TEM grid. The scale bar is 100 nm.

Torr. The growth of HGoRs was started by introducing 7 sccm CH_4 into the chamber, with the H_2 held at 500 sccm, for 35 min. After the reaction, the Cu foils were quickly removed from the hot zone of the CVD furnace using a magnetic rod and permitted to cool to room temperature. Detailed HGoR growth procedures are described in the Supporting Information.

Characterizations. The Raman spectra were measured using a Renishaw Raman RE01 scope with a 514 nm excitation argon laser. SEM characterizations were done using a FEI Quanta 400 ESEM field emission gun at 20 KeV. Transmission electron microscopy (TEM) measurements were performed using a JEOL 2100-F instrument operated at 200 KeV. A 6 probe station (Model FWPX, Desert Cryogenics-LakeShore) was used to measure the electrical properties under vacuum (10^{-5}–10^{-6} Torr). Atomic force microscopy (AFM) images were obtained with a Digital Instruments Nanoscope IIIa in tapping mode, at a scan rate of 1.2 Hz and 512 × 512 resolutions.

RESULTS AND DISCUSSION

After the growth of HGoRs, the samples were transferred onto SiO_2 (100 nm)/Si wafers for further characterizations. Optical microscopy is a useful tool for graphene characterization because graphene areas with different thicknesses can be distinguished by their contrast difference.[26] Figure 1b and c and Figure S1 of the Supporting Information provide several typical optical images of as-produced HGoRs transferred onto SiO_2/Si wafers. In these optical images, one can see that blue graphene ribbon rings concentrically grow upon or under the lighter hexagonal graphene domains to form onion ring like 3D graphene structures. Figure 1b exhibits 7 domains, with graphene domains 1 and 2 and onion domains 1–5, suggesting that the yield of HGoRs is ~70%. This approximate value is consistently observed under the described growth conditions. Graphene domains 1 and 2 are monolayer based on the Raman spectra in Figure S2 of the Supporting Information. In addition, they show a uniform optical contrast, indicating 100% monolayer graphene coverage. Graphene domain 1 was a well-defined hexagon while graphene domain 2 was partially damaged during the transfer process. From Figure 1b, most of the HGoRs (1–4) have the edge-to-edge distances ranging from 70 to 90 μm, suggesting that monolayer graphene domains in HGoRs 1–4 nucleate at similar intervals during the growth process. Through the investigation of 54 HGoRs, ~85% have the edge-to-edge distances ranging from 70 to 90 μm, indicating a narrow size distribution. Meanwhile, a much smaller HGoR 5, with the edge-to-edge distance at ~30 μm, was also observed in Figure 1b, indicating that the monolayer graphene domain in HGoR 5 started growing later than those in HGoRs 1–4. Interestingly, HGoR 5 merged with the adjacent HGoR 1 to form a polycrystalline onion. HGoRs 1–5

dx.doi.org/10.1021/ja403915m | J. Am. Chem. Soc. 2013, 135, 10755–10762

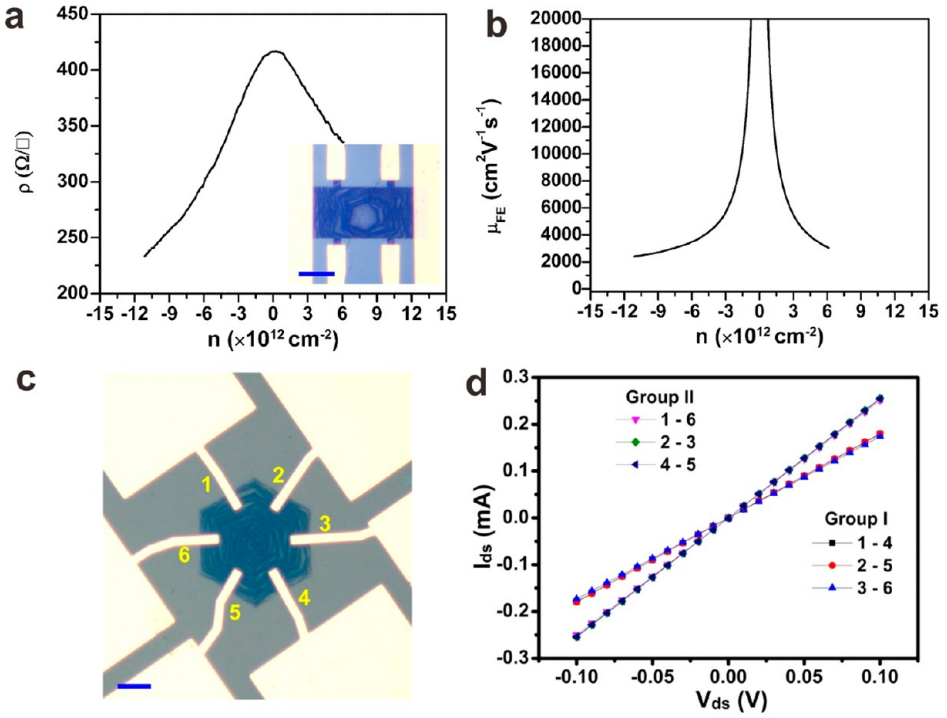

Figure 2. Electrical properties of HGoRs. (a) Resistivity of HGoR as function of carrier density measured at room temperature. The inset is an optical image of the fabricated graphene onion Hall bar field effect transistor on SiO_2/Si substrate; the scale bar is 20 μm. (b) Plot of density-dependent field effect mobility of graphene onion vs carrier density from the device indicated in (a). The field effect mobility was calculated from the Drude model,[29] at a carrier density of 5×10^{12} cm^{-2}, and the mobility was ~4000 cm^2 V^{-1} s^{-1} for the holes, indicative of the high quality of the HGoR. (c) A representative optical image of a fabricated six-terminal device on a SiO_2/Si substrate. The numbers label the device electrodes; the same numbers are used in the $I-V$ curves in (d). The scale bar in (c) is 20 μm. (d) Two-terminal $I-V$ characteristics of the indicated devices in (c) measured at room temperature. The two-terminal $I-V$ curves were measured from two groups, groups I and II. Group I was from the diagonal sides (1–4, 2–5, 3–6), and group II was from the neighboring sides (1–6, 2–3, 4–5). The overlaid $I-V$ characteristics from the two groups indicate that electrical transport through each side of the HGoR was homogeneous. This demonstrates the overall uniformity of the HGoRs. The conductance difference between the two groups was likely due to the difference in device structure.

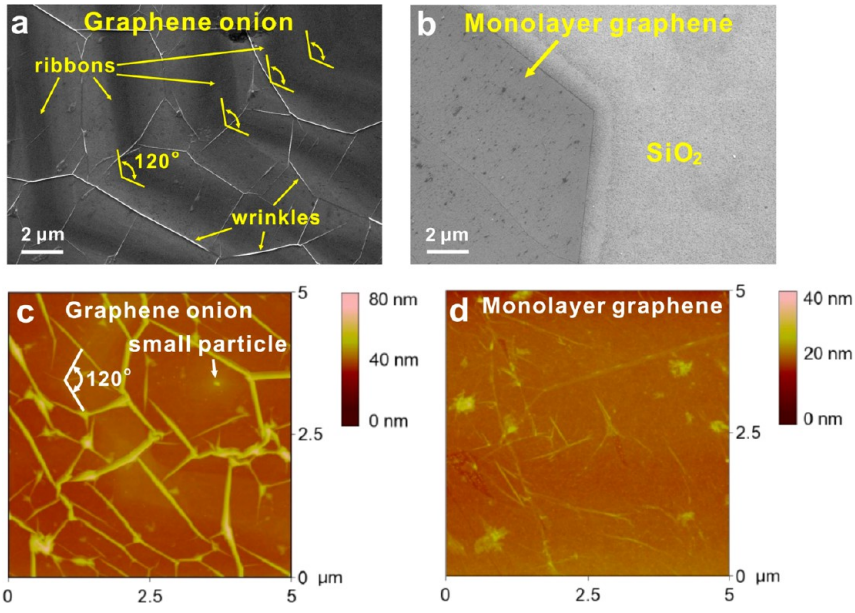

Figure 3. SEM and AFM characterizations of HGoRs transferred onto SiO_2 (100 nm)/Si wafers. (a) A typical SEM image of HGoRs, showing sharp wrinkles and hexagonal ribbons. (b) A typical SEM image of single-crystal hexagonal monolayer graphene domains,[16] demonstrating a flat surface. (c) A typical AFM image of the HGoR, with the height scale bar (right), demonstrating that the root square surface roughness is ~5 nm. The small particle in the middle is the seed that initialized the growth of this particular HGoR. (d) A typical AFM image of monolayer graphene. The root square surface roughness is ~1 nm.

dx.doi.org/10.1021/ja403915m | J. Am. Chem. Soc. 2013, 135, 10755–10762

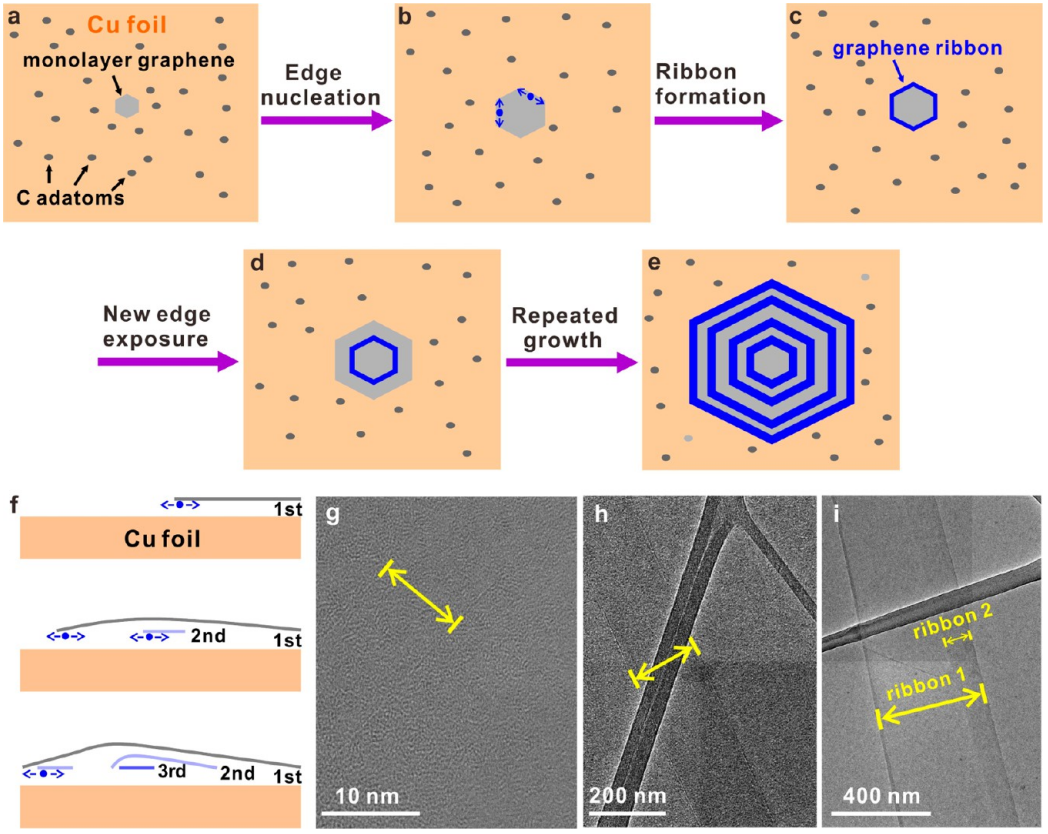

Figure 4. Proposed growth mechanism of HGoRs. (a) A monolayer graphene domain forms on the surface of the Cu foil. (b) New graphene layers nucleate and grow on the edge of the monolayer graphene domain. (c) A one-dimensional hexagonal graphene ribbon ring forms along the edge of the monolayer graphene domain. (d) A new edge was exposed because the monolayer graphene domain grows faster than the underlayers. (e) Repeated growth leads to the final formation of one HGoR. (f) The scheme for the 3D layer-by-layer growth process. The new layer (second) is nucleated on the edge of the topmost (first) layer. The blue dots represent the nucleation site, and the growth direction is indicated by arrows. TEM images of graphene ribbons in HGoRs, with different widths of (g) ~10 nm, (h) ~200 nm, and (i) ~450 nm. (i) demonstrates that ribbon 2 nucleates and grows on the edge of ribbon 1, providing direct evidence of the edge-nucleated 3D growth mechanism.

have distinct innermost graphene ribbon ring sizes, an indication that growth initiation of the innermost graphene ribbon ring was random and different for each HGoR. The ribbons appear more concentric than spiraling. Raman spectroscopy was used to characterize the HGoR shown in Figure 1c. Two points were selected from this HGoR, point A and point B. Figure 1d demonstrates that the middle region (point A) of this HGoR is monolayer and the blue graphene ribbon rings (point B) of this HGoR are multilayer,[27] indicating that the formation of HGoRs is based on the growth of few-layer graphene ribbons on or under monolayer graphene domains. However, as described in the following, few-layer graphene ribbons are revealed to reside on the bottom sides of monolayer graphene domains by H_2SO_4 intercalation experiments and plasma etching studies.

As-produced HGoRs were also transferred onto TEM grids for further characterizations. Figure 1e represents a typical TEM image of a graphene ribbon grown under a suspended graphene film on the TEM grid. From Figure 1e, one can see the graphene ribbon has smooth edges and its width is ~200 nm. Counting the layers at the graphene ribbon's edge indicates that it is tetralayer (see Figure S3a of the Supporting Information). The selected area electron diffraction (SAED) patterns of areas e1 and e2 display typical hexagonal crystalline structures of graphene, confirming graphene films exist at both sides of the graphene ribbon. Interestingly, a slight rotation was observed when overlaying the SAED patterns of areas e1 and e2 (see Figure S3b of the Supporting Information). This slight rotation of SAED patterns was sometimes observed in single-crystal graphene and is suggested to arise from the waviness of the graphene films.[13,28] In this particular case, the regional waviness of the graphene film in Figure 1e could be exacerbated by the graphene ribbon as described below for the wrinkling.

The electrical transport properties were evaluated by fabricating multiterminal devices on HGoRs transferred onto SiO_2/Si wafers (see Supporting Information). The measurements were performed at room temperature under a pressure of less than 10^{-5} Torr. A gating effect was observed on a Hall bar device and is shown in Figure 2a with a mobility of ~4000 $cm^2 V^{-1} s^{-1}$ at a carrier density of 5×10^{12} cm^{-2} based on the Drude model[29] (Figure 2b), indicating the high quality of the HGoR. Additionally, 6 electrodes were patterned on the 6 edges of a HGoR (Figure 2c), which demonstrate the overall uniformity of HGoRs (Figure 2d).

Whether the graphene ribbons reside on the top or the bottom of the hexagonal monolayer graphene domain is critical for understanding the growth mechanism. According to recent research, for bilayer graphene formation on Cu, the secondary layer grows from the Cu side.[30] In this research, we use H_2SO_4 intercalation experiments[31] to further demonstrate that graphene ribbons also reside on the bottom of the hexagonal monolayer graphene domains in this special case (see Figure S4

dx.doi.org/10.1021/ja403915m | J. Am. Chem. Soc. 2013, 135, 10755−10762

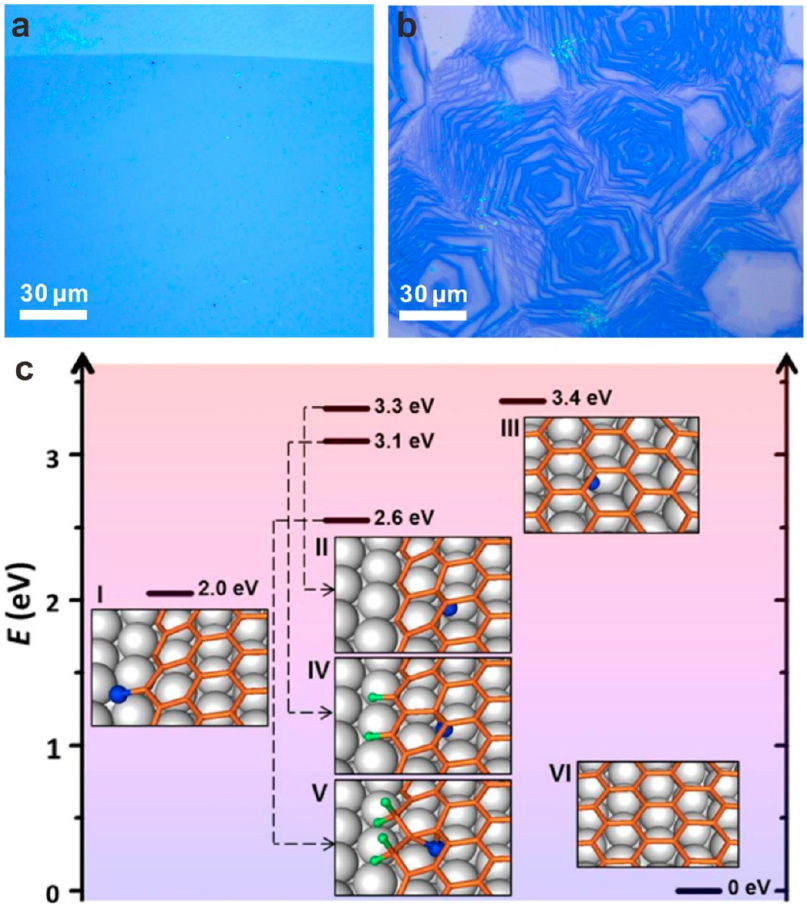

Figure 5. Control experiments and nanoreactor model[14] for graphene nucleation. (a) A continuous monolayer graphene film was obtained after 120 min growth when the H_2 partial pressure was 8.4 Torr (E1 in Table S1 of the Supporting Information). (b) A continuous HGoR film was made after 120 min growth when the H_2 partial pressure was 500 Torr (E2 in Table S1 of the Supporting Information). (c) Energies (shown by bars) and atomic structures of C adatom adsorbed at the intact edge (I), near the intact edge (II), in the interior of graphene (III), and near the hydrogenated sp^2 edge (IV), near the hydrogenated sp^3 edge (V). The energies refer to that of a C atom in graphene on Cu (VI), which is set to zero. The graphene is represented by orange sticks, the Cu substrate by white spheres, and the H in green, and the C adatoms are colored in blue.

of the Supporting Information). H_2SO_4 treatment doped only the top layer hexagonal graphene but did not intercalate between the nanoribbons on the underside. Figure 3a is a typical SEM image of HGoRs transferred onto a SiO_2/Si wafer showing graphene ribbon rings have smooth edges and ∼120° corners. Sharp graphene wrinkles were observed on the surface of the HGoRs. In contrast, a characteristic SEM image of single-crystal hexagonal monolayer graphene[16] transferred onto a SiO_2/Si wafer is shown in Figure 3b, which shows a surface much smoother than that of the HGoR in Figure 3a. This suggests that the graphene ribbons grow on the bottom face of the hexagonal monolayer graphene, which makes the bottom sides wavy. Thus, many sharp wrinkles were produced during the transfer process.

We used AFM to characterize the topology of the HGoRs transferred onto SiO_2/Si wafers (Figure 3c and Figure S5 of the Supporting Information). Figure 3c provides one typical AFM image of the center of a HGoR, showing a graphene ribbon ring overlaid with several sharp graphene wrinkles. A 120° angle indicates the hexagonal shape of the graphene ribbon ring. A section analysis for the same HGoR in Figure 3c is provided in Figure S5 of the Supporting Information, which demonstrates that the height of the graphene ribbon was ∼3 nm, corresponding to the approximate thickness of tetralayer graphene.[32] From Figure S5 of the Supporting Information, we can see heights of graphene wrinkles in HGoRs as high as ∼20 nm. Moreover, several graphene wrinkles crossed the edge of the graphene ribbons without showing sharp discontinuity, which suggests that graphene ribbons were on the bottom of the HGoRs. Figure 3c also shows that the root mean square surface roughness of this HGoR is ∼5 nm. As a comparison, an AFM image of single-crystal monolayer graphene[16] is shown in Figure 3d, indicating a relatively flat surface with its root mean square surface roughness at ∼1 nm. In addition, a small particle was observed in the middle of the HGoR (Figure 3c and Figure S5 of the Supporting Information), with its width being ∼150 nm and its height ∼20 nm, which could be the seed[13] that initialized the growth of this HGoR. Graphene ribbon segments with ∼90° corners were also observed and might originate from the small perturbance of growth environments, such as in the temperature and the flow rate of CH_4, during the growth process. Beyond that suggestion, we do not presently have a rationale for the observation.

The growth of graphene on Cu has been shown to be the direct result of nucleation, growth and coalescence of graphene seeds,[13,14,28] resulting in the formation of polycrystalline graphene films. However, the formation mechanism of HGoRs is distinct from the seed-induced 2D growth. Here we propose an edge-nucleated 3D growth mechanism to explain the formation of HGoRs, as described in Figure 4a–f.

dx.doi.org/10.1021/ja403915m | J. Am. Chem. Soc. 2013, 135, 10755−10762

In the initial growth stage, a monolayer graphene domain nucleates on the Cu surface and gradually grows larger by continuously adding adjacent carbon adatoms (Figure 4a). However, in a hydrogen rich growth environment (see Supporting Information), a new graphene layer could nucleate from the edge of a growing top layer, producing edge nucleation (Figure 4b). The role of hydrogen in the edge nucleation is discussed later (Figure 5 and its related text). The edge-nucleated graphene could evolve to a hexagonal ribbon (Figure 4c) as a result of kinetic factors, which will be discussed later as well. After edge nucleation, new graphene layers start layer-by-layer growth from the bottom side of the previous layer to form few-layer graphene ribbons (Figure 4f and Figure S6 of the Supporting Information). The sizes of the innermost graphene ribbon rings vary (see Figures 1b and c and Figure S1 of the Supporting Information), indicating that the time of activation of the edge of each monolayer graphene domain is random for each HGoR. Meanwhile, monolayer graphene top-layer domains keep growing when new graphene layers nucleate on their edges. Monolayer graphene domains have growth rates higher than those of edge-nucleated, new graphene layers, due to the more efficient contact with the adatom sources, leading to the exposure of new graphene edges (Figure 4d). As the reaction time progresses, new graphene layers nucleate and grow again on the newly exposed edges to form additional hexagonal graphene ribbon rings. After repeated exposure of new monolayer graphene domain edges, more graphene ribbons grow concentrically on the new edges to form HGoRs (Figure 4e and f). Figure S7 of the Supporting Information provides an optical image of one incomplete HGoR, which was occasionally found in the experiments and provides further evidence for the proposed growth mechanism.

The proposed edge-nucleated 3D growth mechanism was further confirmed by TEM characterizations. Figure 4g–i show TEM images of three graphene ribbons on suspended graphene films with widths ranging from 10 to 450 nm, which were randomly found in the HGoR samples. Figure 4g shows that the width of the graphene ribbon is ∼10 nm and it is monolayer, suggesting that this graphene ribbon has just nucleated and it is in the initial growth stage. The graphene ribbon shown in Figure 4h has already grown to ∼200 nm, and it is tetralayer, counting its edge, meaning that more graphene layers would grow on the graphene ribbon via edge nucleation during the extended growth time. Interestingly, two stacked graphene ribbons, ribbon 1 and ribbon 2, were observed in Figure 4i, showing that ribbon 2 grows from the edge of ribbon 1 and providing direct evidence for the proposed edge-nucleated 3D growth mechanism. Meanwhile, Figure S8 of the Supporting Information shows a typical SEM image of HGoRs on the growth substrate, Cu, indicating a weak relation between graphene ribbons and the Cu surface, which excludes the possibility that graphene ribbons nucleate at the sites of the Cu surface features and further confirm the hydrogenation-induced, edge-nucleation growth mechanism.

Why might HGoRs form using these particular conditions? To answer this question, nine experiments (E1–9) to investigate the effects of different growth parameters on the formation of HGoRs were performed and are summarized in Table S1 of the Supporting Information. From Table S1 of the Supporting Information, it can be seen that the growth time, temperature, and CH_4 flow rate have weak influences on the formation of HGoRs. The crucial parameter that determines the formation of HGoRs is the partial pressure of H_2. For example, Figure 5a shows that when the partial pressure of H_2 is ∼8.4 Torr (E1), a uniform monolayer graphene film was obtained after 120 min growth. In contrast, a continuous HGoRs film was obtained while keeping other conditions the same and increasing the partial pressure of H_2 to ∼500 Torr (E2, Figure 5b).

The role of H_2 in the formation of HGoRs can be explained by the nanoreactor model[14] shown in Figure 5c *I*–*V*, which represents the energies of a C adatom at different states, computed from first principles (details can be found in the Supporting Information). The energy of a C atom in graphene on Cu is set to zero (Figure 5c VI). The nucleation of a new graphene layer should start from a single C adatom. It can be adsorbed at the growth front, on the zigzag edge,[14] near the edge, or in the interior of the growing graphene sheet. At low H_2 pressure, the edge exposes pure sp^2 C with one dangling bond for each edge atom. During the growth, the majority of C atoms migrating to graphene will be adsorbed by the free edge (Figure 5c I), leaving very few C adatoms entering underneath graphene (Figure 5c II and III) as a result of their large energy difference of ∼1.4 eV. In this case, the growth of graphene still remains 2D rather than forming a new graphene layer on the original layer. However, at high H_2 pressure, some of the edge C atoms can be hydrogenated.[33−35] The hydrogenation of the growing edge could increase the probability of new graphene layer nucleation near the edge by increasing its affinity for the C adatom. For example, Figure 5c II and V show that hydrogenation would decrease the energy of a C adatom near the edge by ∼0.7 eV, which corresponds to an increase of absorption probability by a factor of $e^{\Delta E/kT} \sim 10^2$ (given a synthesis temperature of ∼1347 K). In this case, the enhanced absorption arises from the hydrogenation-induced sp^3 state of an edge C atom, which forces the neighboring C into the same four coordination state,[36] thus facilitating the adsorption of the C adatom. Overall, it is shown that the hydrogenation of the graphene edge at high H_2 pressure could facilitate the nucleation of the new graphene layer near the growing edge of the previous layer. As the C accumulates around the edge, C clusters[37] would be formed at the edge and a new graphene layer starts to grow. The growth rate is faster along the edge direction (i.e., growth front) of the upper layer than the normal direction. This behavior originates from kinetic factors. Growth along the edge is fed with the accumulated C near the edge. Growth normal to the edge requires the C transport across the edges, where most C would be adsorbed by the outer edges before they arrive at the inner growth front. Therefore, the different C concentrations lead to highly anisotropic growth rates and result in a ribbon like shape. The spacing of the ribbons is determined by the relative rate of nucleation and growth normal to the edge. As more ribbons are formed during the growth, less C is available for inner ribbon growth due to the adsorption of the outer ribbon edges, impeding inner ribbon growth and avoiding the formation of continuous few-layer graphene films. The tilted graphene ribbons were also observed in HGoRs (see Figure S8 of the Supporting Information). This results because, after edge nucleation, the growth between GNRs and top-layer graphene becomes less correlated with each other. This correlation decreases with increasing distance between their growth fronts. The eventual orientations of the growth fronts are determined by the local chemical environment,[14] such as C concentrations, gas fluxes, and temperatures, which are unlikely to be the same for the top-layer graphene and bottomside graphene ribbons.

dx.doi.org/10.1021/ja403915m | J. Am. Chem. Soc. 2013, 135, 10755−10762

Different from general 2D graphene structures, HGoRs have demonstrated two special features due to their 3D structures with modulated thickness. The first feature is that HGoRs could be used to make graphene nanoribbons by using Ar plasma to remove the top-layer, single-crystal, graphene domains (Figure S9 of the Supporting Information). Furthermore, according to other research,[13,14] single-crystal graphene domains made on Cu by CVD show clean zigzag edges. Thus, through further optimizations, this edge-nucleated technique could allow the direct bottom-up growth of graphene nanoribbons with clean edges on Cu substrates, without needing lithography patterns of metal nanowires[22] or organic synthesis procedures.[23] Second, according to recent theoretical research,[38,39] single-layer graphene is not suitable for Li storage because of the weak Li binding energy on a single-layer graphene surface. As shown in Figure S10 of the Supporting Information, according to first-principles calculations, HGoRs could be suitable for Li storage because the Li binding energy between ribbon layers is 1.8 eV, and the Li binding energy at ribbon edges is 3.3 eV, higher than Li cohesive energy (1.6 eV). This feature, though interesting, would be made practical only with suitable scaling.

■ CONCLUSIONS

In this research, although we only demonstrated the synthesis of 3D graphene structures, this edge-nucleated 3D growth method might be generalized to form complex spatial structures from other 2D materials such as h-BN,[40] MoS_2[41] or their hybrids[7] after further optimizations. In conclusion, we report the fabrication of HGoRs on Cu foils. A hydrogenation-induced edge-nucleation 3D growth mechanism was proposed and confirmed by AFM, SEM, Raman spectroscopy, TEM, and first principles calculations.

■ ASSOCIATED CONTENT

Supporting Information

Images, spectra and additional experimental procedures. This material is available free of charge via the Internet at http://pubs.acs.org.

■ AUTHOR INFORMATION

Corresponding Author

yuting@ntu.edu.sg; biy@rice.edu; tour@rice.edu

Notes

The authors declare no competing financial interest.

■ ACKNOWLEDGMENTS

The Singapore National Research Foundation NRF-RF2010-07, the ONR MURI program (00006766, N00014-09-1-1066), AFOSR MURI (FA9550-12-1-0035), Lockheed Martin LANCER IV Program, and AFOSR (FA9550-09-1-0581) provided funding. Computations were performed on NICS Kraken (NSF OCI-1053575), NERSC Hopper (DOE DE-AC02-05CH11231) and DAVINCI (NSF OCI-0959097).

■ REFERENCES

(1) Lee, C.; Wei, X.; Kysar, J. W.; Hone, J. *Science* **2008**, *321*, 385–388.

(2) Novoselov, K. S.; Geim, A. K.; Morozov, S. V.; Jiang, D.; Zhang, Y.; Dubonos, S. V.; Grigorieva, I. V.; Firsov, A. S. *Science* **2004**, *306*, 666–669.

(3) Wang, F.; Zhang, Y.; Tian, C.; Girit, C.; Zettl, A.; Crommie, M.; Shen, Y. R. *Science* **2008**, *320*, 206–209.

(4) Li, X.; Cai, W.; An, J.; Kim, S.; Nah, J.; Yang, D.; Piner, R.; Velamakanni, A.; Jung, I.; Tutuc, E.; Banerjee, S. K.; Colombo, L.; Ruoff, R. S. *Science* **2009**, *324*, 1312–1314.

(5) Bae, S.; Kim, H. K.; Lee, Y.; Xu, X.; Park, J. S.; Zheng, Y.; Balakrishnan, J.; Lei, T.; Kim, H. R.; Song, Y.; Kim, K. S.; Özyilmaz, B.; Ahn, J. H.; Hong, B. H.; Lijima, S. *Nat. Nanotechnol.* **2010**, *5*, 574–578.

(6) Sun, Z.; Yan, Z.; Jun, Y.; Beitler, E.; Zhu, Y.; Tour, J. M. *Nature* **2010**, *468*, 549–552.

(7) Levendorf, M. P.; Kim, C. J.; Brown, L.; Huang, P. Y.; Havener, R. W.; Muller, D. A.; Park, J. *Nature* **2012**, *488*, 627–632.

(8) Haigh, S. J.; Gholinia, A.; Jalil, R.; Romani, S.; Britnell, L.; Elias, D. C.; Novoselov, K. S.; Ponomarenko, L. A.; Geim, A. K.; Gorbachev, R. *Nat. Mater.* **2012**, *11*, 764–767.

(9) Li, Y.; Zhou, W.; Wang, H.; Xie, L.; Liang, Y.; Wei, F.; Idrobo, J. C.; Pennycook, S. J.; Dai, H. *Nat. Nanotechnol.* **2012**, *7*, 394–400.

(10) Zhu, Y.; Li, L.; Zhang, C.; Casillas, G.; Sun, Z.; Yan, Z.; Ruan, G.; Peng, Z.; Raji, A.-R. O.; Kittrell, C.; Hauge, R. H.; Tour, J. M. *Nat. Commun.* **2012**, *3*, 1225.

(11) Chuvilin, A.; Bichoutskaia, E.; Gimenez-Lopez, M. C.; Chamberlain, T. W.; Rance, G. A.; Kuganathan, N.; Biskupek, J.; Kaiser, U.; Khlobystov, A. N. *Nat. Mater.* **2011**, *10*, 687–692.

(12) Sun, Z.; Pint, C. L.; Marcano, D. C.; Zhang, C.; Yao, J.; Ruan, G.; Yan, Z.; Zhu, Yu.; Hauge, R. H.; Tour, J. M. *Nat. Commun.* **2011**, *2*, 559.

(13) Yu, Q. K.; Jaurengui, L. A.; Wu, W.; Colby, R.; Tian, J.; Su, Z. H.; Cao, H.; Liu, Z.; Pandey, D.; Wei, D.; Chung, T. F.; Peng, P.; Guisinger, N. P.; Stach, E. A.; Bao, J.; Pei, S. S.; Chen, Y. P. *Nat. Mater.* **2011**, *10*, 443–449.

(14) Artyukhov, V. I.; Liu, Y.; Yakobson, B. I. *Proc. Natl. Acad. Sci. U.S.A.* **2012**, *109*, 15136–15140.

(15) Sun, Z.; Raji, A.-R. O.; Zhu, Y.; Xiang, C.; Yan, Z.; Kittrell, C.; Samuel, E. L. G.; Tour, J. M. *ACS Nano* **2012**, *6*, 9790–9796.

(16) Yan, Z.; Lin, J.; Peng, Z.; Sun, Z.; Zhu, Y.; Li, L.; Xiang, C.; Samuel, E. L.; Kittrell, C.; Tour, J. M. *ACS Nano* **2012**, *6*, 9110–9117.

(17) Yang, L.; Park, C.-H.; Son, Y.-W.; Cohen, M. L.; Louie, S. G. *Phys. Rev. Lett.* **2007**, *99*, 186801.

(18) Barone, V.; Hod, O.; Scuseria, G. E. *Nano Lett.* **2006**, *6*, 2748–2754.

(19) Jia, X. T.; Campos-Delgado, J.; Terrones, M.; Meunier, V.; Dresselhaus, M. S. *Nanoscale* **2011**, *3*, 86–95.

(20) Kosynkin, D. V.; Higginbotham, A. L.; Sinitskii, A.; Lomeda, J. R.; Dimiev, A.; Price, B. K.; Tour, J. M. *Nature* **2009**, *458*, 872–876.

(21) Jiao, L.; Zhang, L.; Wang, X.; Diankov, G.; Dai, H. J. *Nature* **2009**, *458*, 877–880.

(22) Kato, T.; Hatakeyama, R. *Nat. Nanotechnol.* **2012**, *7*, 651–656.

(23) Cai, J.; Ruffieux, P.; Jaafar, R.; Bieri, M.; Braun, T.; Blankenburg, S.; Muoth, M.; Seitsonen, A. P.; Saleh, M.; Feng, X.; Mullen, K.; Fasel, R. *Nature* **2010**, *466*, 470–473.

(24) Chamberlain, T. W.; Biskupek, J.; Rance, G. A.; Chuvilin, A.; Alexander, T. J.; Bichoutskaia, E.; Kaiser, U.; Khlobystov, A. N. *ACS Nano* **2012**, *6*, 3943–3953.

(25) Lebedeva, I. V.; Popov, A. M.; Knizhnik, A. A.; Khlobystov, A. N.; Potapkin, B. V. *Nanoscale* **2012**, *4*, 4522–4529.

(26) Blake, P.; Hill, E. W.; Neto, A. H. C.; Novoselov, K. S.; Jiang, D.; Yang, R.; Booth, T. J.; Geim, A. K. *Appl. Phys. Lett.* **2007**, *91*, 063124.

(27) Malard, L. M.; Pimenta, M. A.; Dresselhaus, G.; Dresselhaus, M. S. *Phys. Rep.* **2009**, *473*, 51–87.

(28) Li, X.; Magnuson, C. W.; Venugopal, A.; Tromp, R. M.; Hannon, J. B.; Vogel, E. M.; Colombo, L.; Ruoff, R. S. *J. Am. Chem. Soc.* **2011**, *133*, 2816–2819.

(29) Adam, S.; Hwang, E. H.; Galitski, V. M.; Das Sarma, S. *Proc. Natl. Acad. Sci. USA.* **2007**, *104*, 18392–18397.

(30) Nie, S.; Wu, W.; Xing, S.; Yu, Q.; Bao, J.; Pei, S.; McCarty, K. F. *New J. Phys.* **2012**, *14*, 093028.

(31) Dimiev, A.; Bachilo, S. M.; Saito, R.; Tour, J. M. *ACS Nano* **2012**, *6*, 7842–7849.

(32) Rao, C. N. R.; Sood, A. K.; Subrahmanyam, K. S.; Govindaraj, A. *Angew. Chem., Int. Ed.* **2009**, *48*, 7752–7777.

(33) Vlassiouk, I.; Regmi, M.; Fulvio, P.; Dai, S.; Datskos, P.; Eres, G.; Smirnov, S. *ACS Nano* **2011**, *5*, 6069−6076.
(34) Losurdo, M.; Giangregorio, M. M.; Capezzuto, P.; Bruno, G. *Phys. Chem. Chem. Phys.* **2011**, *13*, 20836−20843.
(35) Zhang, W.; Wu, P.; Li, Z.; Yang, J. *J. Phys. Chem. C* **2011**, *115*, 17782−17787.
(36) Boukhvalov, D. W.; Katsnelson, M. I.; Lichtenstein, A. I. *Phys. Rev. B* **2008**, *77*, 035427.
(37) Loginova, E.; Bartelt, N. C.; Feibelman, P. J.; McCarty, K. F. *New J. Phys.* **2008**, *10*, 093026.
(38) Lee, E.; Persson, K. A. *Nano Lett.* **2012**, *12*, 4624−4628.
(39) Liu, Y.; Artyukhov, V. I.; Liu, M.; Harutyunyan, A. R.; Yakobson, B. I. *J. Phys. Chem. Lett.* **2013**, *4*, 1737−1742.
(40) Ci, L.; Song, L.; Jin, C.; Jariwala, D.; Wu, D.; Li, Y.; Srivastava, A.; Wang, Z. F.; Storr, K.; Balicas, L.; Liu, F.; Ajayan, P. M. *Nat. Mater.* **2010**, *9*, 430−435.
(41) Radisavljevic, B.; Radenovic, A.; Brivio, J.; Giacometti, V.; Kis, A. *Nat. Nanotechnol.* **2011**, *6*, 147−150.